The generation of axially aligned seams on triangulated pipe faces

Conference Paper *in* Procedia Engineering · October 2017

DOI: 10.1016/j.proeng.2017.09.784

3 authors:

Harold J. Fogg
Siemens
17 PUBLICATIONS **137** CITATIONS
SEE PROFILE

Jonathan E. Makem
Siemens
34 PUBLICATIONS **152** CITATIONS
SEE PROFILE

Jean Cabello
Siemens
19 PUBLICATIONS **148** CITATIONS
SEE PROFILE

Available online at www.sciencedirect.com

ScienceDirect

Procedia Engineering 203 (2017) 27–39

Procedia Engineering

www.elsevier.com/locate/procedia

26th International Meshing Roundtable, IMR26, 18-21 September 2017, Barcelona, Spain

The generation of axially aligned seams on triangulated pipe faces

Harold J. Fogg[a], Jonathan E. Makem[a], Jean Cabello[b]

Meshing & Abstraction, Digital Factory, Simulation and Test Solutions Siemens PLM Software, SIEMENS.

[a] *Francis House,112 Hills Road, Cambridge, UK. CB2 1PH*
[b] *2000 Eastman Dr., Milford, Ohio 45150 USA*

Abstract

This paper presents a method for creating seams on pipe faces which are effective for reducing the distortion of the face flattening and thus promote the generation of high quality meshes on the faces. The method is applicable to groups of connected B-rep triangulated faces whose underlying surfaces resemble Generalised Cylinders. Isoparametric curves of Generalised Cylinder parametrisations are approximated by establishing singularity-free cross-fields starting with estimated principal curvature directions from which the seams are derived.

Peer-review under responsibility of the scientific committee of the 26th International Meshing Roundtable.

Keywords: seam generation; pipe face; flattening; triangulation parametrisation;

1. Introduction

Piping networks and assemblies comprising many cylindrical surfaces can be found in a huge variety of mechanical devices including automotive and aero-engines, fans, turbines, heating systems etc. In industry an emergent requirement in the modelling and analysis of these geometries is the ability to generate more structured meshes to facilitate structural, CFD and acoustic simulations. For example, accurate contact analysis on cylindrical components is dependent upon well-aligned structured meshes, both axially and circumferentially, on opposite mating surfaces to promote the creation of MPCs and compatible boundary conditions.

1.1. Flattening or parametrisation of triangulated faces

Many face meshing algorithms essentially work in 2-D and for them to be used on a 3-D curved face a flattened representation along with a mapping must be found. This is equivalent to finding a continuous u-v parametrisation over the face. If the face is an analytic or NURBS geometry face then this is already available but if the face is a triangulation it must be computed. If the mesh is generated on the flattened representation with the objective of high quality elements, large distortion in the mapping will adversely affect the qualities of the resulting elements in 3-D. Thus, flattening algorithms are generally designed with the aim of minimising a combination of length, area and

E-mail address: harry.fogg@siemens.com

1877-7058
Peer-review under responsibility of the scientific committee of the 26th International Meshing Roundtable.
10.1016/j.proeng.2017.09.784

angular distortion in the mapping. Other applications include texture mapping, morphing and remeshing. See [1] for a comprehensive survey.

1.2. Flattening of pipe faces

A pipe face is understood here to be a region of a Generalised Cylinder (*c.f.* Sec. 2). For pipe faces a flattening mapping with significantly reduced distortion is often possible by redefining its B-rep to turn its two boundary edge loops into to a single boundary edge loop by introducing a *seam* cut. This is an edge on the face that spans between the two boundary edge loops of the original B-rep and it is included twice with opposite senses in the boundary edge loop of the modified B-rep. This is shown in Fig. 1 and the benefit on mesh quality is clearly demonstrated.

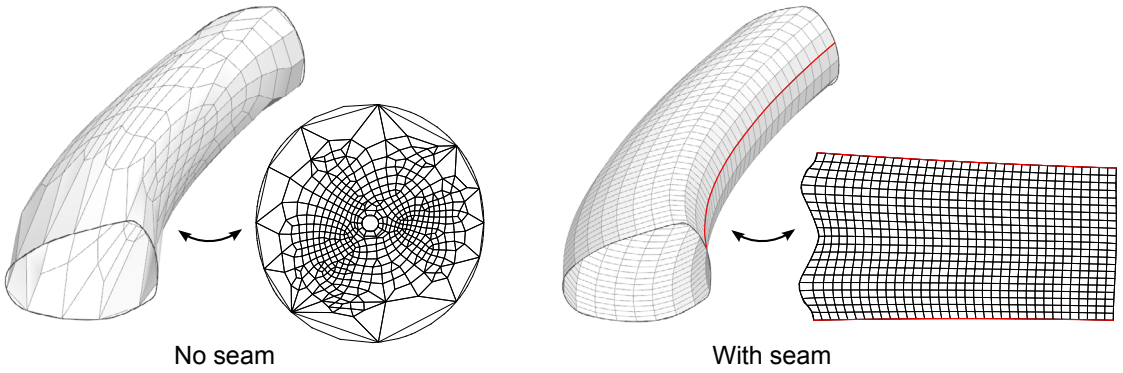

Fig. 1: A 3-D pipe face and its flattened 2-D representations with and without a seam cut, and corresponding sample meshes. These were generated in Simcenter 12 using the flattening method of [2].

1.3. Related work

Various methods have been developed to generate constructive seams on triangulations for parametrisation. Grundig *et al.* [3] proposed a geodesic based algorithm for the particular case of generating optimum seam cuts on architectural textile structures. Guskov *et al.* [4] proposed a method for segmenting a detailed curved triangulation with a net of curves by a process involving mesh simplification and iterative adjustment. Sander *et al.* [5] apply a progressive merging procedure to produce a collection of topological disc charts. Vallet and Levy [6] use a spectral segmentation method to solve for a set of seams which can be manually edited in the event of over segmentation. Campen *et al.* [7] deal with the general problem of generating quantised global parametrisations. Their methods by-pass the need for seams altogether although the techniques involved are complex and require the solution of mixed integer programming problems via clever heuristics to give good performance.

1.4. Contribution

An algorithm is presented that is designed for the particular case of generating effective seams on pipe faces for quad meshing. The approach of establishing a singularity free cross-field starting from approximated principal curvature directions is novel and the value of the approach is supported by theory and by the quality of the resultant quad meshes on the faces.

2. Generalised cylinders

A Generalised Cylinder (GC) is a surface loosely characterised by having a curve in 3-D called an *axis* along which a closed *cross-section* curve is swept to construct the surface. The shape of the cross-section curve may be constant or, more generally, be controlled by a sweeping rule. They cover a wide range of different shapes and their form lends

itself to the intuitive construction of surfaces in computer geometric modelling where they are extensively used. They have been the subject of significant research in computer geometric modelling, computer animation, computer vision, robotics amongst other disciplines, e.g. [8], [9], [10], [11].

A GC with axis $\mathbf{a}$, parametrised by arc length s, and cross-section curve $\mathbf{c}$, parametrised by $\theta \in [0, 2\pi]$, has a standard representation

$$\mathbf{x}(s, \theta) = \mathbf{a}(s) + \mathbf{A}(s)\,\mathbf{c}(\theta), \tag{1}$$

where the sweeping rule is restricted to a linear transformation $\mathbf{A}(s)$. Further constraints are typical and a full taxonomy of GCs with the various permutations of constraints are outlined in [12].

The two most common subclasses are Straight Homogeneous Generalised Cylinders (SHGC) and Planar Right Constant cross section Generalised Cylinders (PRCGC). SHGCs have a planar cross-section curve, a straight axis and a homogeneous scaling as a sweeping rule. This class includes surfaces of revolution.

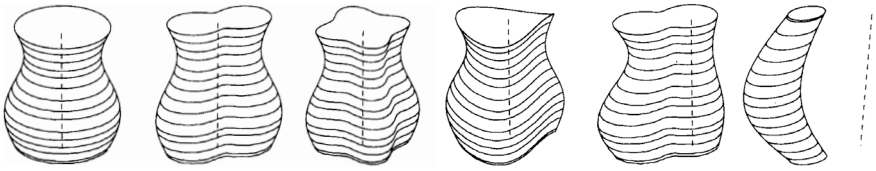

Fig. 2: Example Straight Homogeneous Generalised Cylinders (SHGC), with their cross-sections (θ-isoparametric curves) and axes. Taken from [13].

PRCGCs represent curved pipe-like surfaces. Here the cross section is fixed in size and shape on an orthogonal plane to the axis, which is not necessarily straight. In its standard parametric representation (Eqn. (1)) $\mathbf{A}$ is a special orthogonal (rotation) matrix,

$$\mathbf{A}(s) = \left[\mathbf{a}'(s)\ \mathbf{f}_2(s)\ \mathbf{f}_3(s)\right], \tag{2}$$

which defines a moving frame along the axis, as shown in Fig. 3.

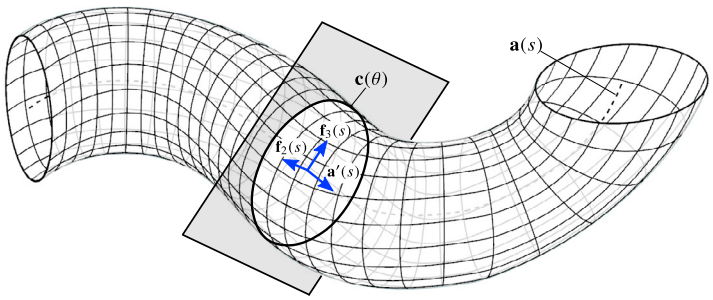

Fig. 3: A Planar Right Constant cross section Generalised Cylinder (PRCGC), with a sample moving frame on the axis, $\mathbf{a}(s)$, corresponding cross-section, $\mathbf{c}(\theta)$, and s- and θ-isoparametric curves.

There remains one degree of freedom for the rotation of the moving frame around $\mathbf{a}'(s)$. The rotation minimising frame (RMF) is the unique frame without intrinsic rotation around $\mathbf{a}'(s)$, thus the tangent vectors of s-isoparametric curves are always parallel to $\mathbf{a}'(s)$. RMF-generated sweeping surfaces are the *de facto* standard for sweep operations in geometric modelling because they have smoother shapes than alternatives in general.

It has been proven for RMF-generated sweeping surfaces (which include PRCFC) that the isoparametric curves are identical to the lines of curvature of the surface [14]. This property does not hold in general. For example, the GC shown in Fig. 4 has a planar cross section but the moving frame has intrinsic rotation about the axis tangent and consequently the lines of curvature deviate from the isoparametric curves, as indicated. For SHGCs only surfaces of rotation will have this line of curvature-isoparametric curve equivalence.

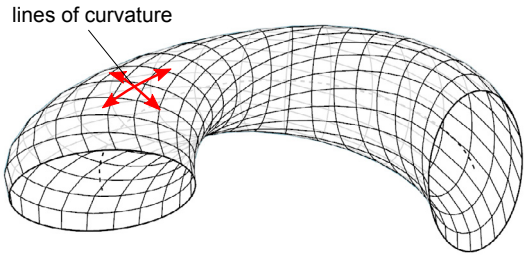

Fig. 4: A Generalised Cylinder with a constant planar cross section but the moving frame has intrinsic rotation about the axis tangent.

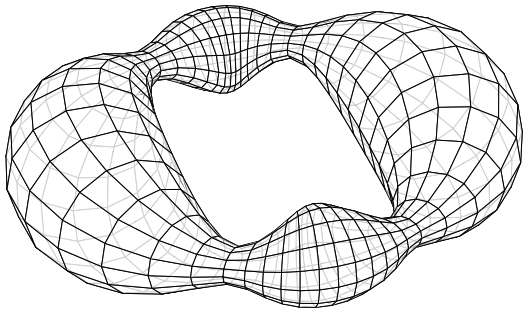

Fig. 5: A canal surface generated by a sphere of varying radius moving along a circular axis. Taken and adapted from [15].

Canal surfaces are a related class surfaces that can represent many common curvy pipes. They are formed by the envelope of a family of spheres of variable radius with their centres on an axis curve. An example is shown in Fig. 5. If the axis curve is planar then, again, isoparametric curves are identical to the lines of curvature. If not, then the radius must vary in particular ways according to the torsion and curvature of the axis to have this property [16].

3. High level discussion

3.1. Recognising the need for seams

Faces that could take a canonical GC or canal surface parametrisation are deemed to be good candidates for the introduction of seams. Recognising if this is possible on a faceted face is not trivial. A series of heuristics are used for adequately completing this task including least square (ls-)fitting of regular cylinders and cones to the triangulation vertices, assessing the shapes of the boundary closed loops in consideration of the surface normals and gauging the contours of the implicit underlying surface. The details will not be covered here.

3.2. Seam shape

Observing that if the surface can be parametrised as a GC or a canal surface and the target mesh is all-quad then, most usually, the grid of isoparametric curves describes a mesh with desirable element qualities. Thus, it should be possible to produce a mesh which is similar by applying a seam cut along a θ-isoparametric curve and generating a transfinite grid on the flattened representation, which would be expected to be close to a regular rectangle (as in Fig. 1 (right)). The aim then is to reverse engineer a smooth θ-isoparametric curve to use as a seam when the actual parametrisation isn't available.

3.3. Overview of seam solution method

The essential strategy for solving a seam on a 2-loop face involves approximating the principal curvature directions of the surface. These are assumed to almost point along the isoparametic directions of a canonical GC parametrisation of the surface. Next, two orthogonal *quasi* isoparametic direction fields are established from the principal curvature directions. The quasi θ- and s-isoparametic directions will be referred to as *axis* and *circumferential* directions respectively. Finally, a streamline of the axis direction field is numerically traced between the two loops. This is illustrated in Fig. 6.

As explained in Sec. 2, the assumption of line of curvature-isoparametric curve equivalence is only correct for certain subclasses of GCs. However, it has been found that for a wide variety of surfaces the same strategy will produce well-shaped useful seams. In Fig. 6 the algorithm has been applied to a GC. Some irregularity in the principal curvature direction field is noticeable near the left hand boundary loop where the curvature is umbilical (*i.e.* the pricipal curvatures are identical). This can also occur in the vicinity of G^1 and G^2 discontinuities of a surface. To produce a consistent isoparametric direction field a smoothing stage is required to eliminate such irregularities.

3.4. Handling N-loop pipe faces and inner loops

For a pipe face with N-loops and $N > 2$ the $N - 2$ inner loops are automatically tessellated over with approximate G^1 continuity using the Parasolid faceting toolkit [17] to produce a 2-loop face. Thereafter, the standard process applicable to 2-loop faces is used to solve a single seam across the face between the two boundary loops. Finally, the inner loop fill-in tessellations are removed which may divide the seam into separate portions if the seam path happens to travel through the filled in inner loop. This is illustrated in Fig. 7.

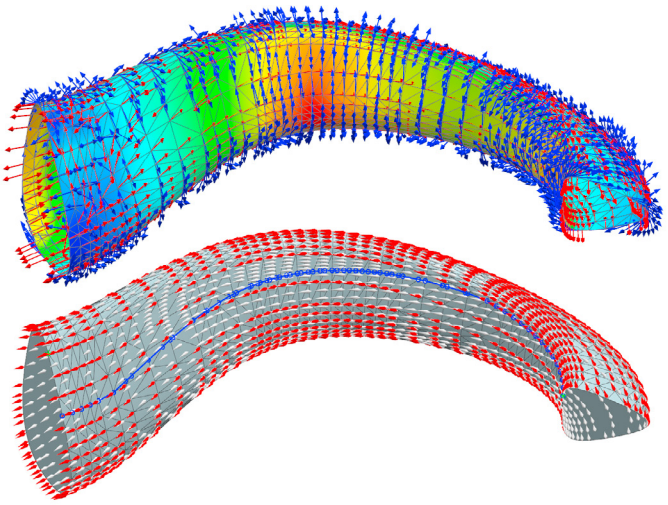

Fig. 6: Contour plot of the first principal curvature of a GC surface and red and blue vectors indicating the first and second principal curvature directions respectively (above). Established axis directions and numerically traced streamline (in blue) (below).

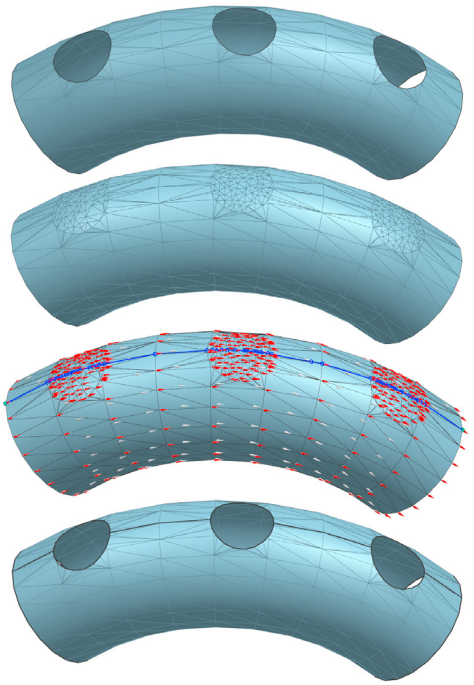

Fig. 7: Process for faces with inner boundary loops.

4. Curvature estimation

A method was implemented for numerically approximating surface curvature on linear triangulations based on the work of [18] and [19]. The approach makes local estimates at vertices by solving a ls-best-fit local quadratic height function to the 1-rings of vertices and their normals. Then analytic formulae are used to determine the principal curvatures and directions of the quadratic height functions.

5. Cross-field theory

The lines of curvature of a G^2 continuous surface away from umbilical points describe an orthogonal grid. A cross-field or 4-way rotationally symmetric (4-RoSy) vector field [20] that is free from singularities can be used to represent their tangent directions.

5.1. Representation

A piecewise discrete representation of a cross-field on a triangulation involves the following attributes:

vertex	edge
1. A surface normal, $\mathbf{n}$. 2. A cross reference vector, $\mathbf{d}$ – one of the 4 equivalenced 3-D unit vectors spread at $\pi/2$ intervals on the surface normal's tangent plane.	1. The change in angle of the cross-field across the edge, $\Delta\theta$. 2. The matching, m, between the cross reference vectors at the end vertices – integer in $\{0, 1, 2, 3\}$.

For an edge between vertices labelled 1 and 2, as illustrated in Fig. 8, after first rotating the cross reference vector of 1 to the tangent plane of 2, $\mathbf{d}_1 \rightarrow \mathbf{d}'_1$, then

$$\mathbf{d}_2 = \mathbf{R}\Big((\Delta\theta + m\pi/2)\mathbf{n}_2\Big)\mathbf{d}'_1, \tag{3}$$

where $\mathbf{R}(\cdot *)$ denotes a rotation of $\cdot$ about the axis $*$.

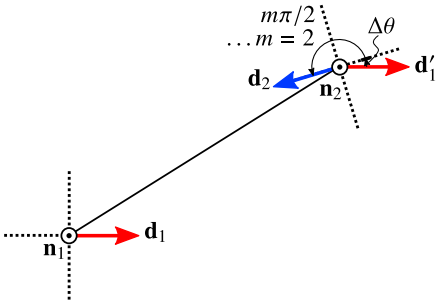

Fig. 8: Change in angle and matching of cross-field across edge.

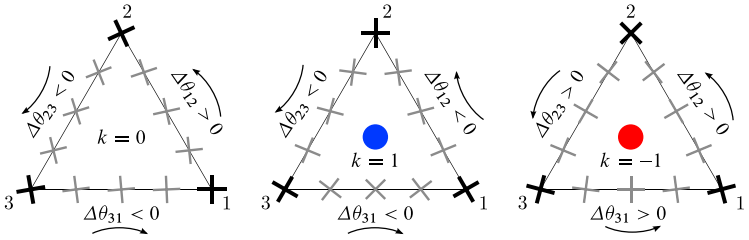

Fig. 9: Cross-field singularity indices inside triangles. Taken from [21].

5.2. Determining optimum change in angles and matchings

The optimum matching that gives the least change in angle of the cross-field across the edge can be computed by

$$m^* = \text{round}\,(\theta_{12}/2\pi) \tag{4}$$

$$\Delta\theta^* = \theta_{12} - m^*\pi/2 \tag{5}$$

where θ_{12} is the positive angle between $\mathbf{d}'_1$ and $\mathbf{d}_2$ in range $[0, 2\pi)$.

5.3. Singularities

Singularities occur in the cross-field at points around which the net change in angle of the cross-field is a multiple of $\pi/2$ other than zero. The enclosed net singularity index of a triangle with vertices labelled 1, 2, 3 is

$$k = -\frac{\Delta\theta_{12} + \Delta\theta_{23} + \Delta\theta_{31}}{\pi/2} \tag{6}$$

Cross-field singularities are illustrated in Fig. 9.

5.4. Smoothing

Smoothing of a cross-field involves reducing rapid changes and potentially lowering the number of singularities that occur. Optimising the matchings and angles of a cross-field is a mixed-integer programming type problem [22], which is expensive to solve. Fortunately, methods have been devised to avoid consideration of the integer matching parameters and to optimise by minimising continuous objective functions.

Algorithm 1 `Smooth cross`

Find new $\mathbf{d}_i$ of central vertex i:
$\mathbf{v}_{\text{rosy}\,i} = \{\}$
for vertex in 1-ring **do**
  $\mathbf{d}_j \rightarrow \mathbf{d}'_j$ ... proj. or rotate onto plane $\mathbf{n}_i$
  Compute $\theta_{\text{rosy}\,j}(\mathbf{d}'_j)$
  Compute $\mathbf{v}_{\text{rosy}\,j}(\theta_{\text{rosy}\,j})$
  $\mathbf{v}_{\text{rosy}\,i}$+= $\mathbf{v}_{\text{rosy}\,j}$
Normalise($\mathbf{v}_{\text{rosy}\,i}$)
Compute $\theta_{\text{rosy}\,j}(\mathbf{v}_{\text{rosy}\,i})$
$\theta_i = \theta_{\text{rosy}\,j}/4$
Compute $d_i(\theta_i)$

Algorithm 2 `Boundary-aligned initialisation of cross-field`

alive ← boundary vertices with assigned cross reference vectors
narrowband ← non-boundary neighbours of boundary vertices
while !*narrowband*.empty **do**
  v_0 = *narrowband*.pop()
  SmoothCross(v_0) ... Alg. 1 where uninitialised $\mathbf{d}_i$s are neglected.
  for v_1 in 1-ring of v_0 **do**
    if v_1 is not in *alive* **then**
      narrowband.insert(v_1)

Hertzmann *et al.* [23] devised a function for measuring the distortion between N-way rotationally symmetric vectors (cross-field $\Rightarrow N = 4$) which is invariant to the choice of equivalenced vectors. Using an arbitrary reference axis and measuring the angles of reference vectors from it, the distortion between 1 and 2 is measured by

$$\xi(\theta_1, \theta_2) = \tfrac{1}{2}(1 - \cos(N(\theta_1 - \theta_2))), \tag{7}$$

with the range $[0, 1]$ from perfectly aligned to misaligned by π/N. This is a non-linear function with respect to the angles, so a non-linear solver is needed to minimise an objective function that uses it.

An alternative method that involves only linear operations is to use Palacios *et al.'s* [20] *RoSy representation vectors*, $\mathbf{v}_{\text{rosy}}$. These are unit vectors that are functions of the cross reference vectors which are invariant to the selection of the equivalenced reference vector. In terms of angle from an arbitrary axis they are given by

$$\theta_{\text{rosy}} = N\theta \bmod 2\pi = N(\theta + M\pi/2) \bmod 2\pi \quad | \, M \in \mathbb{Z}, \tag{8}$$

where θ is the angle of a cross reference vector. A very simple scheme to smooth the cross of a vertex using RoSy representation vectors is given in Alg. 1.

6. Establishing axis directions

We seek a cross-field on a pipe face whose flow lines can be decomposed into two families that approximate s- and θ- isoparametric curves of a GC parametrisation. A cross-field is initialised on a pipe face by estimating its curvature and setting one of the obtained principal directions as a cross-field direction. The cross-field can only be decomposed into two families of 2-way rotationally symmetric vector fields if it is singularity free.

Typically, the maximum absolute curvature value direction will correspond to the circumferential direction and the minimum corresponds to the axis direction. However, this may not be the case if the axis curve is highly curved or the cross-section changes rapidly. Fillets, for example, have them the other way around. Therefore the axis directions are not determined based on the magnitude of the principal curvature values.

6.1. Solution method

The developed method for determining the axis directions is as follows:

1. Estimate curvature at each vertex and set the cross-direction as one of the principal curvature directions.
2. Set the optimum change in angle and matchings for each edge.
3. Determine the enclosed net singularity index for each triangle.
4. If the singularity index of each triangle is not zero then smooth cross-field. A basic smoothing algorithm is used where each vertex is visited once and its cross reference vector is optimised by Alg. 1 and then the changes in angle and matchings of the edges are recomputed. This repeated until all singularities have been removed or

until a maximum number of iterations is exceeded (5 is used), in which case the determination of axis directions is aborted.

5. The two families of orthogonal 2-way rotationally symmetric vector fields are established from the singularity-free cross-field. Figure 10 (left) shows a discrete cross-field on a triangulation. It is singularity-free so Eqn. (6) is zero and therefore the sum of the matchings (± according to edge sense) is 0 mod 4 for every triangle.

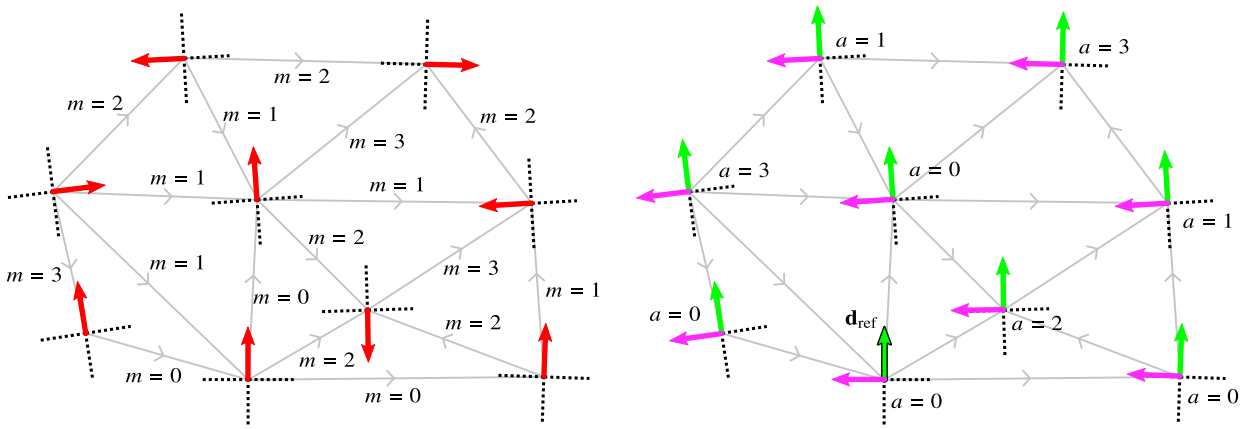

Fig. 10: Singularity-free cross-field (cross reference vectors, $\mathbf{d}_i$ in red) (left) and a pair of orthogonal continuous vector fields, $\mathbf{u}_1$ (in green) and $\mathbf{u}_2$ (in pink) (right).

Starting from a reference vertex (index 0 is used) the matchings of the cross-directions relative to it, a, for all other vertices are calculated by a marching method starting at the reference vertex and spreading to all other vertices. The relative matchings between neighbouring vertices i and j across an edge ij are related by

$$a_j = (a_i - m_{ij}) \bmod 4. \tag{9}$$

A pair of orthogonal continuous vector fields are then implicitly solved as

$$\mathbf{u}_k = \mathbf{R}\left((a_i + k - 1)\frac{\pi}{2}\mathbf{n}_i\right)\mathbf{d}_\mathbf{i} \quad | \quad k \in \{1, 2\} \tag{10}$$

as shown in Fig. 10 (right). The pair of orthogonal 2-way rotationally symmetric vector fields are related as plus-minus these vector fields.

6. Distinguishing which vector field corresponds to the axis and which to the circumferential directions is done as follows: Approximate the shortest path between the loops of the pipe, measure the misalignment between it's tangent directions and the (2-way rotationally symmetric) vector fields and select the one of the two with the lowest misalignment value. The shortest path is approximated by the shortest path of the graph defined by the triangulation edges and is solved by the Dijkstra method with multiple sources and multiple targets as the triangulation vertices of the loops. Tangent vectors at segment junctions of the shortest path are calculated as the average of the segment displacement vectors and misalignment between the tangent vectors and the 2-way rotationally symmetric vector fields are calculated by Eqn. (7) with $N = 2$.

An example of the axis directions solved on a swept face of circular profile and convex and concave fillet faces is shown in Fig. 11.

Fig. 12 shows results for a face composed of a merged cylinder and convex fillet. Their interface is a G^2 discontinuity so the estimated curvature directions are unstable (Fig. 12 (above)). But smoothing effectively irons out the disorder and a well-shaped axis direction field can then be solved (Fig. 12 (below)).

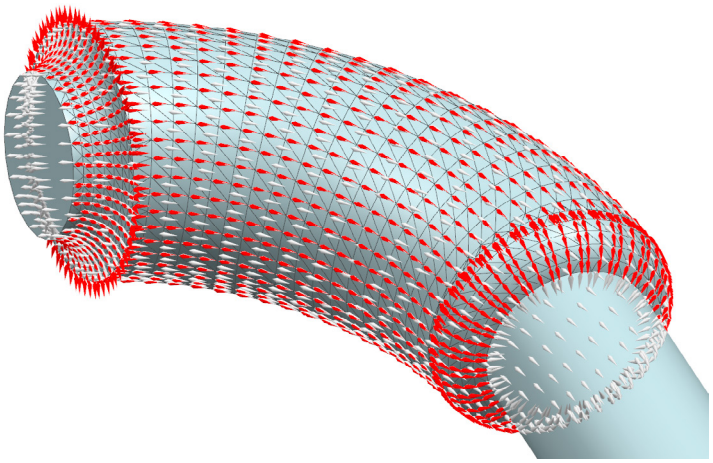

Fig. 11: Axis directions example.

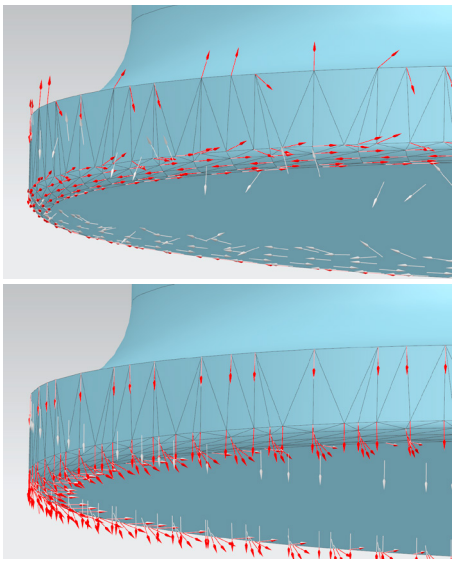

Fig. 12: The cross reference vectors from curvature estimation (above) and the axis direction field solved after smoothing the initial cross-field (below).

6.2. *Initialising cross-field from boundaries*

In umbilical regions where the normal curvature is close to being symmetric (*i.e* $\kappa_1 \sim \kappa_2$) the principal curvature directions are unstable. For example, the face shown in Fig. 13 is a truncated sphere so the initial curvature-based cross-field is disorganised (Fig. 13 (left)) (The apparent partial order is a consequence of the specifics of the curvature estimation numerical algorithm and the triangulation.) Although smoothing can eliminate all singularities the flow

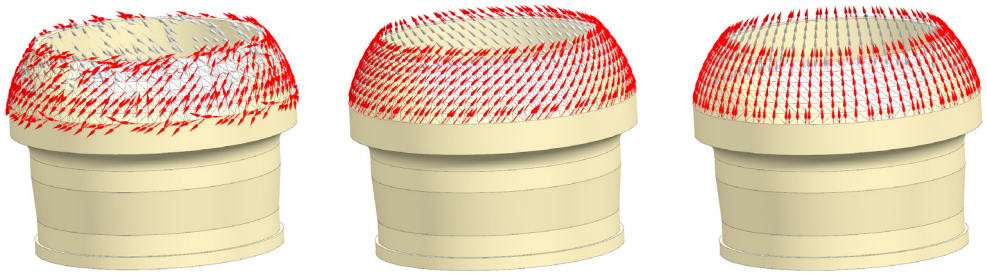

Fig. 13: Initial curvature-based cross reference vectors (left) and corresponding solved axis directions after smoothing (middle). Axis directions solved from initial boundary-aligned cross-field (right).

lines spiral instead of travelling along great circles between the loops, as would the θ-isoparametric curves of a GC parametrisation (Fig. 13 (middle))

In these cases another cross-field initialisation strategy is used. It starts with with boundary-aligned cross reference vectors and these are propagated to the interior. The simple algorithm that is used is described in Alg. 2. This algorithm usually produces cross-fields with good properties for our purposes on umbillical pipe faces, as demonstrated in Fig. 13. However, there is a dependency on the boundary loops being roughly aligned with the circumferential directions.

7. Solving seams

Parametrising the surface *à la* Campen *et al.* [7] *etc.* is certainly an option for generating a quad mesh and seam using the established singularity-free cross-field. An alternative approach is described here that is lightweight in comparison and produces consistent reliable results, satisfying the user requirement for an axially aligned seam on the pipe face – a hitherto missing component of the meshing workflow in Simcenter 12.

7.1. Edge-Only seam solution method

Dijkstra's method is used to find an edge-only seam solution on pipe faces. A shortest path is solved over the triangulation edge graph from a starting vertex of one loop to the nearest vertex of the other loop. For generalised cylinders with straight axes and low levels of rotation of the moving frame a plain Dijkstra's method using geometric edge lengths will produce reasonably shaped seams. But to produce seams with more favourable shapes in general the edge lengths are biased according to the axis directions that have been solved over the face. The benefit of this step is demonstrated in Fig. 14 (left).

Lengths are assigned to edges of the graph based on a combination of geometric length, l_{ij}, and the misalignment of the edge with the axis directions, ϵ_{ij},

$$\bar{l}_{ij} = l_{ij} + r\epsilon_{ij}, \tag{11}$$

where r is a weighting constant. The edge misalignment with the axis directions is computed by

$$\epsilon_{ij} = \frac{\xi(\measuredangle \mathbf{u}_{ij}\mathbf{d}_i, 0) + \xi(\measuredangle \mathbf{u}_{ij}\mathbf{d}_j, 0)}{2}, \tag{12}$$

where $\mathbf{u}_{ij}$ is the unitised displacement vector of the edge and ξ is the cross misalignment formula Eqn. (7) with $N = 2$.

7.2. Continuous seam solution method

Constraining the seam to travel along triangulation edges can lead to sharp kinks when the triangulation locally does not have edges that are aligned with the axis directions. To get by this problem another method is used to trace a streamline of the axis direction field freely across triangles. The disadvantage is that the triangulation will have to be adjusted to include edges along the seam solution. The method for tracing streamlines over the triangulation is based on [24] which is efficient and robust.

7.3. Contingency seam solution

In cases where the method fails to establish a singularity free cross-field and therefore a consistent set of axis and circumferential directions is unattained, the contingency solution is to use a plain Dijkstra method to generate the seam. On the rare occasion where this occurs it usually means that the face is grossly different from a recognisable pipe face and consequently it is not a good candidate for seam creation.

8. Connected aligned seams on groups of connected pipe faces

8.1. Connected pipe faces

For a series of connected pipe faces needing seams it is beneficial to have their respective seams line up to avoid splitting the edge loops shared between adjacent pipe faces more than once. If the pipes are connected in a non-manifold configuration then the first step is to divide them into manifold groups. In the manifold groups a loop of edges may be all adjacent to a single face if they are all *free* edges, or adjacent to two faces if they are all *internal* edges. Therefore, there are just two possibilities of pipe face connectivity graphs: a *loop* where every edge loop is connected to two pipe faces (*e.g.* Fig. 15) and a *line* which is similar except for two edge loops that are connected to a single pipe face (*e.g.* Fig. 14 (right)).

8.2. Strategy for generating connected aligned seams

The strategy for generating aligned seams is to order the solution of seams on the pipe faces of the groups. The method starts at a chosen *seed* point on one of the loops and a priority queue is initialised with its adjacent faces. It proceeds by solving the seam on the next face in the priority queue, traced from the seam point on one of its loops and creating a new seam point on the opposite loop. The priority queue is appended to afterwards with the un-seamed faces adjacent to the loop where the just-solved seam terminated. Priority in the queue is according to the LILO scheme with the modification that faces not needing seams (such as planar annuli) are given the lowest priority.

8.3. Choice of seed point

The initial seed point is chosen with preferences for vertices connected to pre-existing seams, vertices connected to frozen edges and vertices connected to the most edges. The choice has an impact on the result; it affects the side of the pipe face that the seam is created on and if the Edge-Only solution method is used it can have a large bearing on the shape quality of the generated seam depending on the nature of the triangulation. If a single face is being handled then there is scope for optimising the seed vertex choice either by trial-and-error or by a more sophisticated algorithm. But when there are multiple connected pipe faces and their seams are required to line up and attach to each other the co-dependency of seam solutions on the faces following from the initial choice of seed vertex means that optimising the seed vertex is a demanding problem. Therefore it is difficult to avoid kinks occurring in an Edge-Only seam of a particular face because attempting to move the seam to another side where the triangulation is more favourable would entail moving all other seams of the other connected faces. For this reason the default procedure used on connected pipe faces is to chose one initial seed point and employ the Continuous method for generating the seam on all of the faces.

8.4. Special case treatment of near-planar faces

Since near planar faces don't need seams and axis directions may not be readily established a special case solution method is employed for them. Firstly, it is checked if there is an existing seam point on the opposite loop, in which case the seam for the face travels straight to that point. It does not matter if the if this seam is degenerate as it will not be generated. If there is no existing seam point on the opposite loop then the seam is solved as the shortest path to the opposite loop.

9. Seam solution examples

The resulting aligned seams of the algorithm using Edge-Only and Continuous tracing methods are are shown in Fig. 14. The superiority of the Edge-Only seam solution method with axis alignment biasing over a plain Dijkstra method is clearly demonstrated in 14 (left). In Fig. 14 (right) a comparison of the Edge-Only and Continuous seam solutions on the same group of pipe faces is shown. For the lower pipe faces of the group the seams produced by the two methods are identical because some pragmatic tolerance based vertex snapping is incorporated into the Continuous method. The deviation of the two on the faces higher up in the group occurs as a consequence of the triangulation not containing edges that are sufficiently in-line with the solved axis direction of the faces. In deciding which tracing method to use the relative importance of retaining an unaltered triangulation and creating well-shaped seams without kinks must be considered.

Fig. 15 shows the aligned seam solution on the faces of a hollow pipe body and a swept hex mesh. It is important in the swept hex mesh generation algorithm for the seams on the inner and outer pipe faces of the body to be 'opposite' each other. Hence, the Continuous tracing method is used as it will more reliably achieve this regardless of the triangulation details.

A showcase of aligned seams on groups of pipe faces and all-quad meshes is shown in Fig. 16.

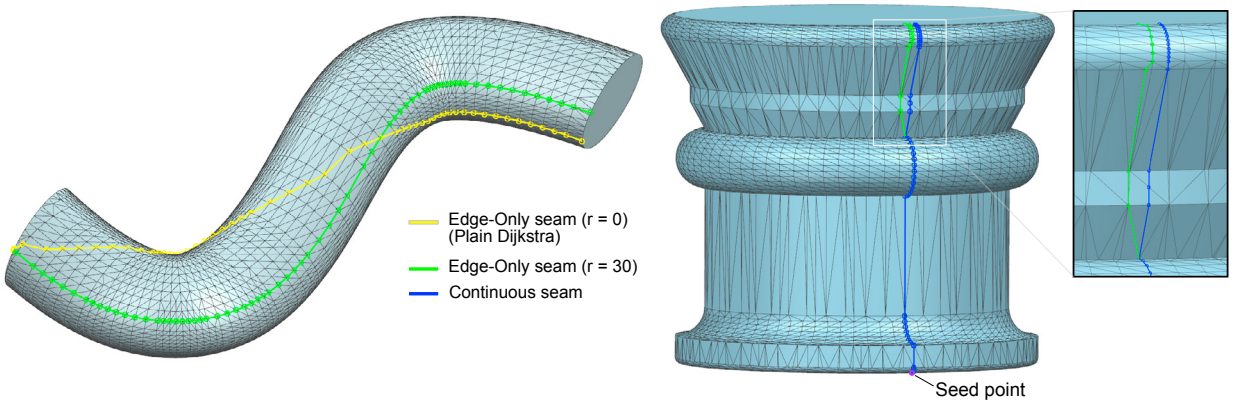

Fig. 14: A comparison of seam solutions: Seams solutions on a PRCGC using the Edge-Only method with and without the axis alignment edge length scaling (left). A connected aligned seam solution on a group of pipe faces using the Edge-Only and Continuous tracing methods (right).

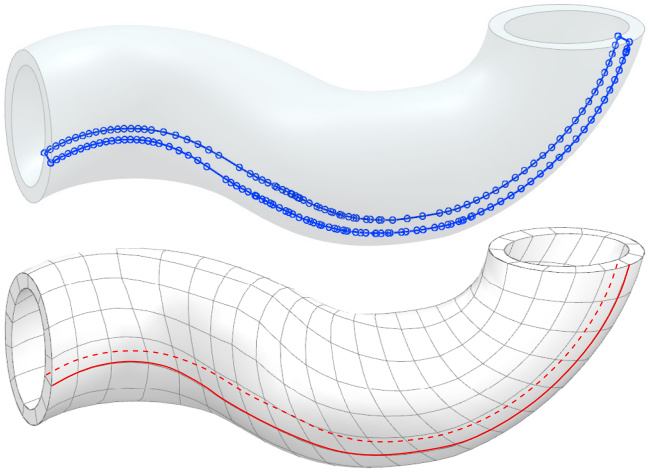

Fig. 15: Aligned seam solution on the faces of a hollow pipe body (above) and a swept hex mesh (below).

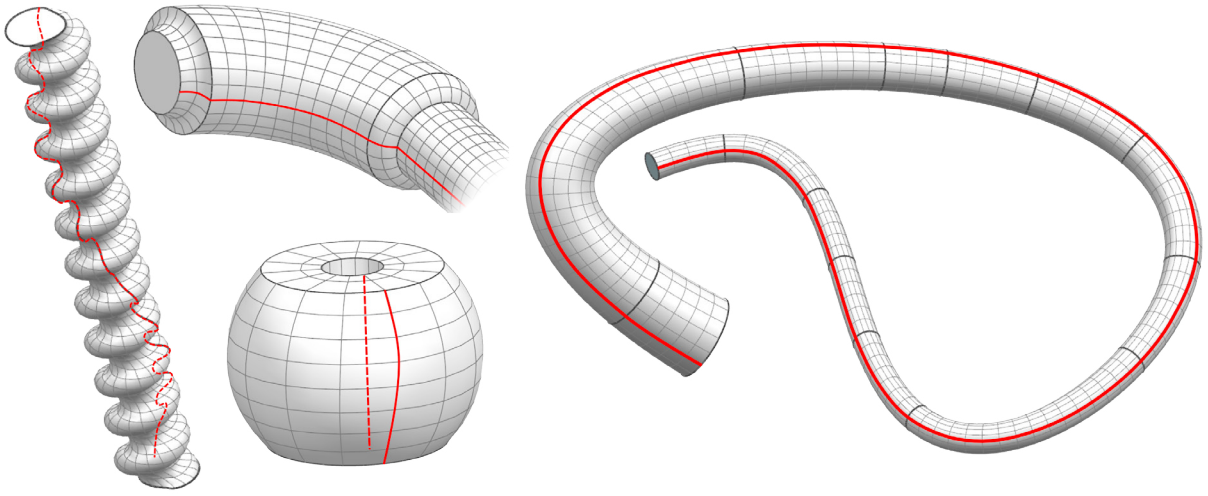

Fig. 16: A showcase of aligned seams on groups of pipe faces and all-quad meshes.

10. Conclusion

The rationale and technical details of an algorithm for generating effective seams on pipe faces has been presented. The method has been implemented in Simcenter 12 [25] as an improvement to its seam generation technology. A Cartesian Slabbing algorithm has also been developed which uses the seams to generate meshes with high degrees of axial alignment on pipe faces [26].

11. Acknowledgements

The authors thank Mary Otte manager of the Meshing & Abstraction Group, Simcenter, Siemens PLM, for her support and encouragement in doing this work.

References

[1] K. Hormann, K. Polthier, A. Sheffer, Mesh parameterization: Theory and practice, in: ACM SIGGRAPH ASIA 2008 Courses, SIGGRAPH Asia '08, ACM, New York, NY, USA, 2008, pp. 12:1–12:87. doi:10.1145/1508044.1508091.
[2] K. Beatty, N. Mukherjee, Flattening 3d triangulations for quality surface mesh generation, in: Proceedings of 17th International Meshing Roundtable, 2008, pp. 125–139.
[3] L. Grundig, E. Moncrieff, P. Singer, D. Strobel, High-performance cutting pattern generation of architectural textile structures, in: Fourth International Colloquium on Computation of Shell & Spatial Structures, 2000.
[4] I. Guskov, K. Vidimče, W. Sweldens, P. Schröder, Normal meshes, in: Proceedings of the 27th Annual Conference on Computer Graphics and Interactive Techniques, SIGGRAPH '00, ACM Press/Addison-Wesley Publishing Co., New York, NY, USA, 2000, pp. 95–102. doi:10.1145/344779.344831.
[5] P. V. Sander, J. Snyder, S. J. Gortler, H. Hoppe, Texture mapping progressive meshes, in: Proceedings of the 28th Annual Conference on Computer Graphics and Interactive Techniques, SIGGRAPH '01, ACM, New York, NY, USA, 2001, pp. 409–416. doi:10.1145/383259.383307.
[6] B. Vallet, B. Lvy, What you seam is what you get, Tech. rep., INRIA - ALICE Project Team (2009).
[7] M. Campen, D. Bommes, L. Kobbelt, Quantized global parametrization, ACM Trans. Graph. 34 (6) (2015) 192:1–192:12. doi:10.1145/2816795.2818140.
[8] H. Rom, G. Medioni., Part decomposition and description of 3d shapes, in: Proceedings of International Conference on Pattern Recognition, 1994, pp. 629–632.
[9] M. soo Kim, E. joo Park, H. yong Lee, Modeling and animation of generalized cylinders with variable radius offset space curves, The Journal of Visualization and Computer Animation 5 (1994) 189–207.
[10] A. Gross, Analyzing generalized tubes, in: Proceedings of SPIE - The International Society for Optical Engineering, 1997. doi:10.1117/12.189111.
[11] R. T. Farouki, K. M. Nittler, Rational swept surface constructions based on differential and integral sweep curve properties, Computer Aided Geometric Design 33 (2015) 1 – 16. doi:10.1016/j.cagd.2014.09.004.
[12] S. A. Shafer, T. Kanade, The theory of straight homogeneous generalized cylinders, Tech. rep. (1983).
[13] F. Ulupinar, R. Nevatia, Shape from contour: straight homogeneous generalized cylinders and constant cross section generalized cylinders, IEEE Transactions on Pattern Analysis and Machine Intelligence 17 (2) (1995) 120–135. doi:10.1109/34.368175.
[14] C. Maurer, B. Juttler, Rational approximation of rotation minimizing frames using pythagorean-hodograph cubics, J. GEOM. GRAPHICS 3 (2) (1999) 141–159.
[15] A. Gray, E. Abbena, S. Salamon, Modern Differential Geometry of Curves and Surfaces with Mathematica, Third Edition (Studies in Advanced Mathematics), Chapman & Hall/CRC, 2006.
[16] Y. Y. Fatih Dogan, The relation between parameter curves and lines of curvature on canal surfaces, Tech. rep., arXiv:1203.4604 (2012).
[17] Parasolid PLM Components, `https://www.plm.automation.siemens.com` (Accessed 19-May-2017).
[18] D. Wang, B. Clark, X. Jiao, An analysis and comparison of parameterization-based computation of differential quantities for discrete surfaces, Comput. Aided Geom. Des. 26 (5) (2009) 510–527. doi:10.1016/j.cagd.2009.02.006.
[19] X. Jiao, H. Zha, Consistent computation of first- and second-order differential quantities for surface meshes, in: Proceedings of the 2008 ACM Symposium on Solid and Physical Modeling, SPM '08, ACM, New York, NY, USA, 2008, pp. 159–170. doi:10.1145/1364901.1364924.
[20] J. Palacios, E. Zhang, Rotational symmetry field design on surfaces, ACM Trans. Graph. 26 (3). doi:10.1145/1276377.1276446.
[21] H. J. Fogg, C. G. Armstrong, T. T. Robinson, Automatic generation of multiblock decompositions of surfaces, International Journal for Numerical Methods in Engineering 101 (13) (2015) 965–991, nme.4825. doi:10.1002/nme.4825.
[22] D. Bommes, H. Zimmer, L. Kobbelt, Mixed-integer quadrangulation, ACM Trans. Graph. 28 (3) (2009) 77:1–77:10. doi:10.1145/1531326.1531383.
[23] A. Hertzmann, D. Zorin, Illustrating smooth surfaces, in: Proceedings of the 27th Annual Conference on Computer Graphics and Interactive Techniques, SIGGRAPH '00, ACM Press/Addison-Wesley Publishing Co., New York, NY, USA, 2000, pp. 517–526. doi:10.1145/344779.345074.
[24] M. Dorobantu, Efficient streamline computations on unstructured grids, Tech. rep. (1997).
[25] Siemens Simcenter 3D, `www.plm.automation.siemens.com/en_us/products/simcenter/3d/modeling/index.shtml`, (26-May-2017).
[26] N. Mukherjee, J. E. Makem, A cartesian slab based multiblocking strategy for irregular cylindrical surfaces, submitted to the 26th International Meshing Rountable (2017).